Volume 22
Number 20
28 May 2024
Pages 3997-4192

Organic & Biomolecular Chemistry

rsc.li/obc

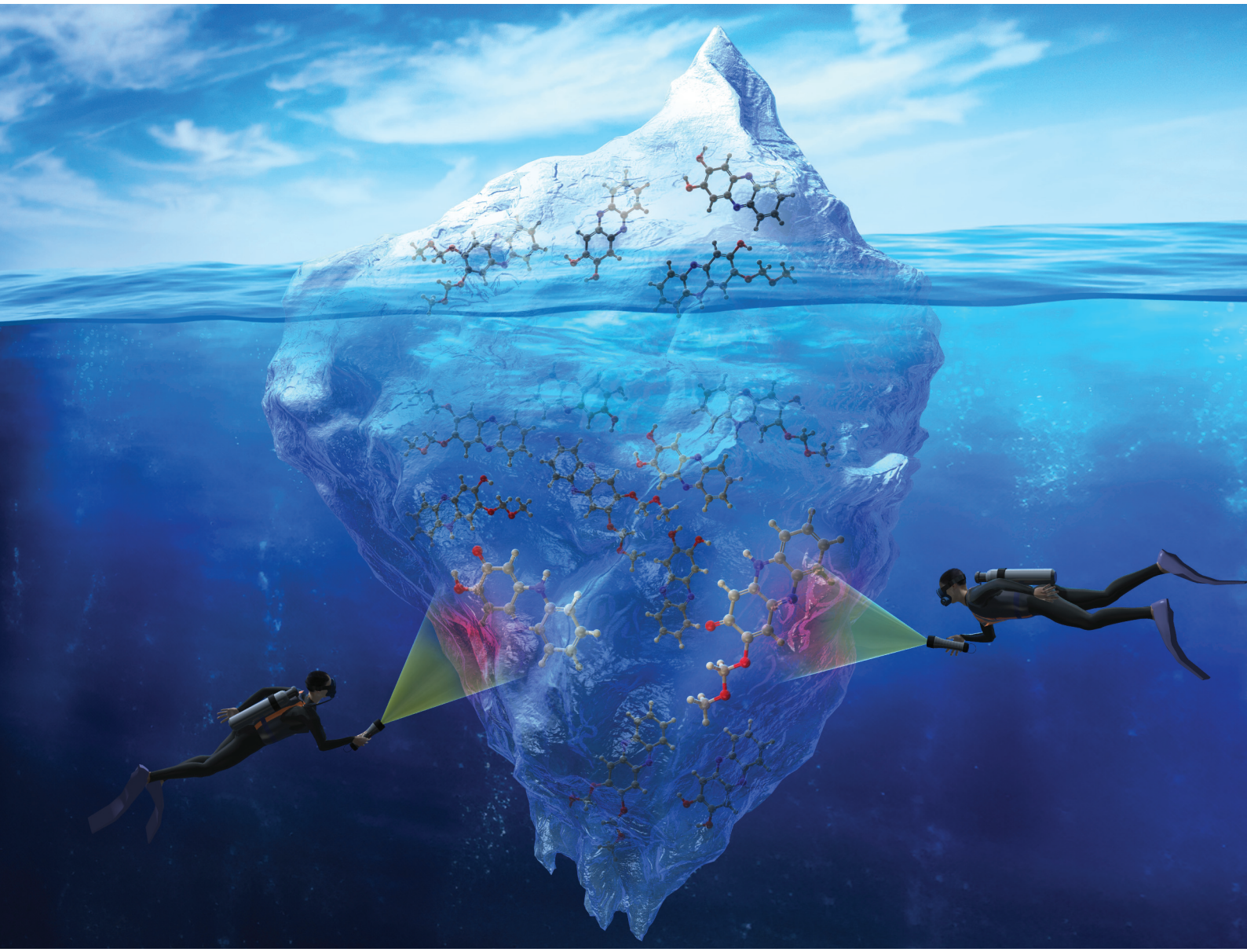

ISSN 1477-0520

ROYAL SOCIETY OF CHEMISTRY

PAPER

Yousuke Ooyama *et al.*

Photochromism of phenazine-2,3-diol derivatives through excited state intermolecular proton transfer based on keto–enol tautomerization

Organic & Biomolecular Chemistry

ROYAL SOCIETY OF CHEMISTRY

PAPER

View Article Online
View Journal | View Issue

Cite this: *Org. Biomol. Chem.*, 2024, **22**, 4077

Photochromism of phenazine-2,3-diol derivatives through excited state intermolecular proton transfer based on keto–enol tautomerization†

Kazuki Ohira, Kumpei Kozuka, Naoki Kaneda, Masahiro Yamamoto, Keiichi Imato and Yousuke Ooyama *

Photochromism through excited-state intermolecular proton transfer (ESInterPT) processes based on keto–enol tautomerization was found in phenazine-2,3-diol **PD1** and its monoalkoxy derivative **PD2** in a glassy matrix at 77 K: the colorless solutions of enol forms **PD1-E** and **PD2-E** at 298 K transformed into orange-colored solutions of keto forms **PD1-K** and **PD2-K** upon photoirradiation (λ = 385 nm) at 77 K. Furthermore, this report is the first to achieve the single-crystal X-ray structural analyses of phenazine-2,3-diol **PD1** and its monoalkoxy derivative **PD2**, since the report on the synthesis of **PD1** 70 years ago. Indeed, it was found that **PD1** and **PD2** molecules exist in the keto form (**PD1-K**) and the enol form (**PD2-E**), respectively, in the crystal, and the neighboring **PD1-K** and **PD2-E** molecules are linked by one-dimensional intermolecular NH···O and OH···N hydrogen bonding, respectively. The fact suggests strongly that for **PD1** and **PD2**, the formation of continuous intermolecular hydrogen bonding in aggregates such as in a glassy matrix at 77 K is involved in the keto–enol tautomerization of phenazine-2,3-diol derivatives based on ESInterPT. More interestingly, the color and the photoabsorption spectrum of the solids obtained by sublimation of crystals of **PD2-E** are similar to those for the crystals of **PD1-K**, indicating that the **PD2** molecule exists in the keto form (**PD2-K**) in the solid of the sublimate. Therefore, this study provides a valuable insight for a greater understanding of the keto–enol tautomerization of diazaacene-diol derivatives and their photophysical properties in the solution and in the solid state.

Received 9th March 2024,
Accepted 10th April 2024

DOI: 10.1039/d4ob00387j

rsc.li/obc

Introduction

Excited-state proton transfer (ESPT)[1] is a fundamental process in chemistry and biology that has gained significant attention due to its diverse applications,[2] including in white light-emitting diodes (LEDs),[3] light-driven proton pumps by bacteriorhodopsin,[4] and fluorescent protein-based biosensors for cation detection.[5] From a molecular structure perspective, the ESPT process can be classified into intramolecular and intermolecular proton transfer processes (ESIntraPT and ESInterPT, Scheme 1). In most cases, these processes are caused by tautomer species possessing different electron density distributions such as keto–enol tautomerization.[6] If the keto–enol tautomerization based on the ESPT processes occurs in a chromophore, such a dye molecule can induce a color change due to alternation of the π electronic state, that is, so-called photochromism. In addition, tautomerization in a fluorophore often induces a significant redshift in the fluorescence wavelength, leading to a substantial Stokes shift (SS) in the range of 6000–12 000 cm^{-1}. However, the ESIntraPT process requires the presence of intramolecular hydrogen bonding between proton donor and acceptor groups, that is, it is limited to molecules containing 5- or 6-membered ring hydrogen bonding structures, such as 3-hydroxyflavone,[7] 2-hydroxybenzophenone,[8] and 2-(2′-hydroxyphenyl)benzothiazole (Scheme 1a).[9] On the other hand, the ESInterPT process has been found in molecules without 5- or 6-membered ring hydrogen bonding structures, including 3-hydroxy-2-naphthanilide,[10] lumazine,[11] anthracen-2-yl-3-phenylurea,[12] 7-hydroxyquinoline,[13] 7-azaindole,[14] and 2-hydroxyphenazine (Scheme 1b and c).[15] Among them, Ogawa *et al.* revealed that 2-hydroxyphenazine exhibits photochromic properties by ESInterPT:[15] when a 2-methyltetrahydrofuran (2-MeTHF) solution containing 2-hydroxyphenazine was irradiated with UV light at 365 nm at 77 K, a new photoabsorption band appeared in the long-wavelength region (*ca.* 450–600 nm) with a decrease in the absorbance of the short-wavelength photoabsorption

Applied Chemistry Program, Graduate School of Advanced Science and Engineering, Hiroshima University, 1-4-1 Kagamiyama, Higashi-Hiroshima 739-8527, Japan. E-mail: yooyama@hiroshima-u.ac.jp

† Electronic supplementary information (ESI) available. CCDC 2328436, 2328438, 2328440 and 2328442. For ESI and crystallographic data in CIF or other electronic format see DOI: https://doi.org/10.1039/d4ob00387j

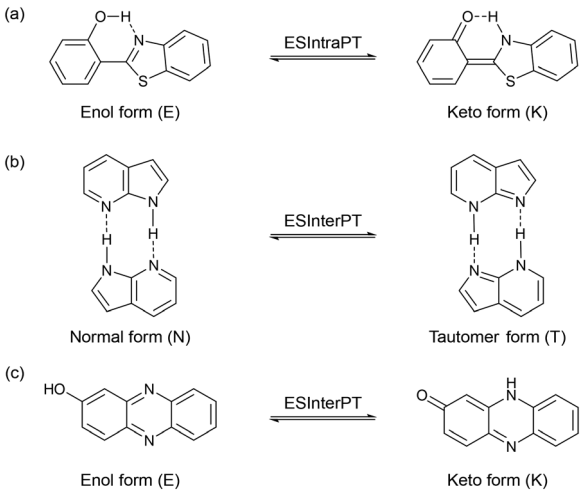

Scheme 1 Schematic representation of (a) ESIntraPT for 2-(2′-hydroxyphenyl)benzothiazole, (b) ESInterPT for 7-azaindole, and (c) ESInterPT for 2-hydroxyphenazine.

band (*ca.* 400–450 nm). Indeed, the color changes from pale yellow to purple-red with UV light irradiation. They proposed that the color change was due to the ESInterPT from the enol (E) to the keto (K) forms in hydrogen-bonded aggregates, because the long-wavelength photoabsorption bands are assigned to the keto (K) form (Scheme 1c). Moreover, it has been reported that the keto–enol tautomerization of 7-hydroxyquinoline (7HQ) takes place through the ESPT along a hydrogen-bonded ammonia wire and a hydrogen-bonded alcohol chain which is mediated by protic solvent molecules.[16] However, studies based on experimental data for photochromism through the ESInterPT process are limited.

In our previous study,[17] we designed and developed phenazinone derivatives **PZ1** and **PZ2** having a similar structure to the keto form of phenazine-2,3-diol **PD1** and its monoalkoxy derivative **PD2**, respectively (Fig. 1 and 2). It was found that in THF, **PZ1** and **PZ2** exhibited an intense photoabsorption band (photoabsorption maximum λ_{max}^{abs} = *ca.* 480 nm and the molar extinction coefficient (ε) = *ca.* 11 000 M^{-1} cm^{-1}) originating from the phenazinone skeleton, while **PD1** showed a weak photoabsorption band with an ε of *ca.* 1700 M^{-1} cm^{-1} at around 480 nm which is assigned to the formation of phenoxide ions by the partial deprotonation of the hydroxy groups.[18]

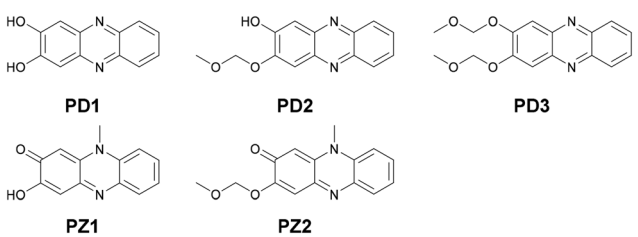

Fig. 1 Chemical structures of phenazine-2,3-diol derivatives **PD1–3** and phenazinone derivatives **PZ1** and **PZ2**.

Fig. 2 Enol and keto forms of **PD1** and **PD2**.

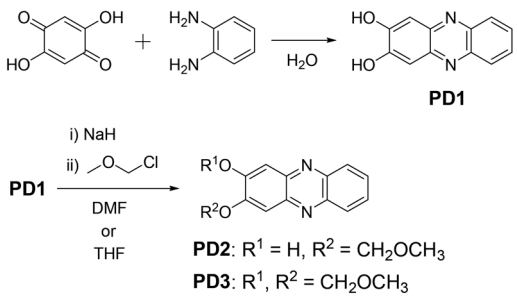

Scheme 2 Synthetic routes to **PD1–3**.

This decisive result inspired us to explore the possibility of ESPT in phenazine-2,3-diol derivatives which would offer an important insight into the photochromism of diazaacene-diols such as diaza-naphthalene and diaza-anthracence derivatives with two hydroxy groups.

For this purpose, in this study, we performed photoabsorption and fluorescence spectral measurements of phenazine-2,3-diol derivatives **PD1–3** in solution, a glassy matrix at 77 K, and the solid state, in comparison with those of phenazinone derivatives **PZ1** and **PZ2** (Fig. 1 and Scheme 2, see the ESI† for a detailed synthetic procedure). It is expected that **PD1** and **PD2** with hydroxy groups will exhibit photochromic properties based on keto–enol tautomerization similar to 2-hydroxyphenazine possessing ESInterPT, whereas **PD3** without hydroxy groups does not show such photochromic characteristics. Meanwhile, this report is the first to achieve the single-crystal X-ray structural analyses of **PD1** and **PD2**, although the synthesis of **PD1** was reported 70 years ago and its characterization was finally determined by NMR spectral analysis 15 years ago.[19] Indeed, it was found that the **PD1** molecule exists in the keto form (**PD1-K**) in the crystal, but the **PD2** molecule exists in the enol form (**PD2-E**) in the crystal (Fig. 2). Herein, we report an investigation of the photochromic properties of **PD1** and **PD2** through the ESInterPT processes based on keto–enol tautomerization.

Results and discussion

Optical properties

The photoabsorption and fluorescence spectra of **PD1–3**, **PZ1**, and **PZ2** in THF are shown in Fig. 3, and their optical data are summarized in Table 1. **PD1–3**, **PZ1**, and **PZ2** showed a moder-

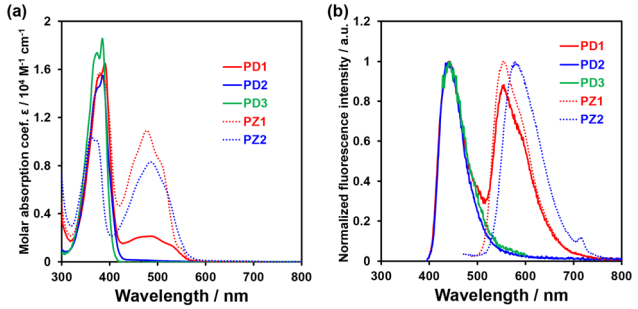

Fig. 3 (a) Photoabsorption and (b) fluorescence (λ^{ex} = 390 nm for **PD1**, 385 nm for **PD2**, 385 nm for **PD3**, 378 nm for **PZ1**, and 361 nm for **PZ2**) spectra of **PD1–3**, **PZ1**, and **PZ2** (1.0×10^{-4} M) in THF.

Table 1 Optical data of **PD1–3**, **PZ1**, and **PZ2** in THF

Dye	λ_{max}^{abs}/nm (ε/M^{-1} cm^{-1})	λ_{max}^{fl}/nm (Φ_{fl}[a])	τ_{fl}[b]/ns
PD1	390 (17 500)	440, 555 (<0.02)	2.13, 3.54[c]
	480 (1700)	558 (0.09)	2.89[d]
PD2	385 (15 500)	443 (<0.02)	2.41[c]
PD3	385 (16 500)	443 (<0.02)	2.70[c]
PZ1[e]	378 (15 700)	554 (003)	3.40[d]
	478 (10 900)		
PZ2[e]	361 (10 500)	579 (0.04)	3.26[d]
	487 (8300)		

[a] Fluorescence quantum yields (λ^{ex} = 390 nm and 480 nm for **PD1**, 385 nm for **PD2**, 385 nm for **PD3**, 378 nm for **PZ1**, and 361 nm for **PZ2**) were determined using a calibrated integrating sphere system. [b] Fluorescence lifetimes. [c] Photoexcited at 366 nm. [d] Photoexcited at 451 nm. [e] In our previous study.[17]

ate and narrow photoabsorption band (λ_{max}^{abs} = 361–390 nm and an ε of *ca.* 10 500–17 500 M^{-1} cm^{-1}), which is assigned to the $S_0 \rightarrow S_3$ ($\pi\pi^*$) transition originating from the phenazine skeleton or a partial phenazinone skeleton through time-dependent density functional theory (TD-DFT) calculations (Fig. 16, Table S13, and Fig. S26†) as discussed later. Moreover, **PD1**, **PZ1**, and **PZ2** exhibited another λ_{max}^{abs} at longer wavelength regions: a broad photoabsorption band with an ε of 1700 M^{-1} cm^{-1} at 480 nm for **PD1**, an ε of 10 900 M^{-1} cm^{-1} at 478 nm for **PZ1**, and an ε of 8300 M^{-1} cm^{-1} at 487 nm for **PZ2**. The TD-DFT calculations revealed that for **PZ1** and **PZ2**, the photoabsorption band in longer wavelength regions is due to the $S_0 \rightarrow S_1$ ($\pi\pi^*$) transition originating from the phenazinone skeleton (Table S13 and Fig. S26†). On the other hand, for **PD1**, the weak photoabsorption band at around 480 nm is ascribable to the formation of phenoxide ions by the partial deprotonation of the hydroxy groups (Fig. 5).[17,18] Indeed, as evidence of the formation of phenoxide ions, for **PD1**, an increase in the absorbance at around 480 nm was observed with increasing water content in the THF solution (Fig. 4a); meanwhile, when water was added to the THF solution of **PD2**, a photoabsorption band appeared at 480 nm and the absorbance increased with the increase in water content (Fig. 4b). On the other hand, such a photoabsorption spectral change was not

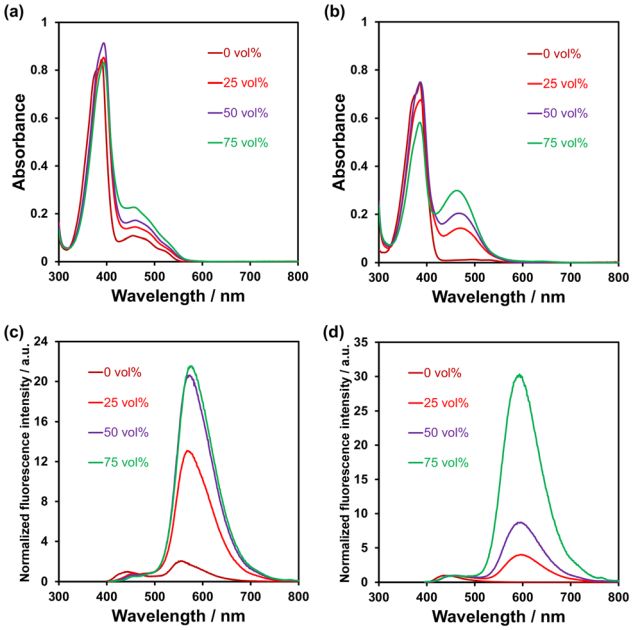

Fig. 4 Photoabsorption spectra of (a) **PD1** and (b) **PD2** (5.0×10^{-5} M) in THF containing water (0–75 vol%). Fluorescence spectra (λ^{ex} = 390–394 nm for **PD1** and 386–387 nm for **PD2**) of (c) **PD1** and (d) **PD2** (5.0×10^{-5} M) in THF containing water (0–75 vol%).

observed upon addition of water to the THF solution of **PD3** (Fig. S30a†). Moreover, for the DMSO solution of **PD1** and **PD2**, the photoabsorption band at around 480 nm increased upon addition of NaOH aq. and decreased upon addition of HCl aq. (Fig. S28d and S29d†), which suggests an increase and a decrease in phenoxide ions, respectively. On the other hand, such a photoabsorption spectral change was not observed in the DMSO solution of **PD3** upon addition of HaOH aq. or HCl aq. (Fig. S30c†). Evidently, these results indicate that the enhancements of the absorbance at around 480 nm upon the addition of water to the **PD1** and **PD2** solutions are attributed to the formation of the phenoxide ion species **PD1-P** and **PD2-P** with the partially deprotonated hydroxy moiety (Fig. 5), as discussed later in ^{1}H NMR spectral measurements. Thus, for **PD1**, the reasonable reason for the appearance of the photoabsorption band originating from the phenoxide ions in absolute THF could be attributable to the contribution of **PD1-P′** with intramolecular hydrogen bonding and/or intramolecular proton transfer (Fig. 5a), leading to stabilization of the phenoxide species by charge dispersion.[20]

In the corresponding fluorescence spectra upon photoexcitation (λ^{ex}) at 361–390 nm (Fig. 3b), **PD1**, **PD2**, and **PD3**

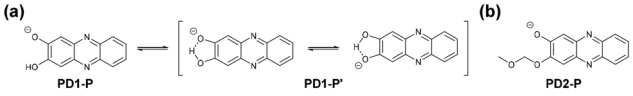

Fig. 5 Chemical structures of phenoxide ions (a) **PD1-P**, **PD1-P′**, and (b) **PD2-P**.

showed a fluorescence maximum (λ^{fl}_{max}) at around 440 nm originating from the phenazine skeleton, and **PZ1** and **PZ2** showed a λ^{fl}_{max} at around 554–579 nm originating from the phenazinone skeleton. It should be noted here that **PD1** exhibited another fluorescence band with λ^{fl}_{max} at 555 nm and its fluorescence intensity increased with increasing water content in THF solution (Fig. 4c), as in the case of photoabsorption spectra. Similarly, for **PD2**, the appearance of a fluorescence band with λ^{fl}_{max} at 579 nm upon addition of water to the THF solution and the enhancement of fluorescence intensity with the increase in water content were observed (Fig. 4d). Furthermore, for **PD1** in THF with and without water and **PD2** in THF with water, fluorescence bands at 550–580 nm were also observed with λ^{ex} at 480 nm for **PD1** and at 463–497 nm for **PD2** (Fig. S28 and S29†). Therefore, based on these results, the fluorescence bands of **PD1** and **PD2** at 550–580 nm can be assigned to fluorescence emission originating from their phenoxide species **PD1-P** (**PD1-P′**) and **PD2-P** (Fig. 5). Interestingly, the fluorescence quantum yields ($\Phi_{fl} \leq 0.04$ for **PD2**, **PD3**, **PZ1** and **PZ2**) for the fluorescence band originating from the phenazine or phenazinone skeleton are considerably lower than that ($\Phi_{fl} = 0.09$ for **PD1**) for the fluorescence band originating from phenoxide species (Table 1). Furthermore, the formation of the phenoxide ion species **PD1-P** and **PD2-P** with the partially deprotonated hydroxy moiety, that is, the existence of the enol (**PD1** and **PD2**)–phenoxide ion (**PD1-P** and **PD2-P**) equilibrium is evident from the temperature-dependent photoabsorption and fluorescence spectral measurements of **PD1–3** in 2-methylTHF (2-MeTHF). For the solutions of **PD1** and **PD2**, the photoabsorption and fluorescence bands originating from phenoxide species in a longer wavelength region decrease with decreasing temperature, but for **PD3**, the photoabsorption and fluorescence bands originating from the phenazine skeleton monotonically increase with increasing temperature (Fig. S32–S34†).

The time-resolved fluorescence lifetime measurements demonstrated that the fluorescence lifetime (τ_{fl}) values of **PD1–3**, **PZ1**, and **PZ2** were estimated to be 2.13 ns (λ^{fl}_{max} = 440 nm) and 3.54 ns (λ^{fl}_{max} = 555 nm) with λ^{ex} at 366 nm and 2.89 ns (λ^{fl}_{max} = 558 nm) with λ^{ex} at 451 nm for **PD1**, 2.41 ns (λ^{ex} = 366 nm) for **PD2**, 2.70 ns (λ^{ex} = 366 nm) for **PD3**, 3.40 ns (λ^{ex} = 451 nm) for **PZ1**, and 3.26 ns (λ^{ex} = 451 nm) for **PZ2** (Table 1 and Fig. S35†). The fact clearly indicates that the phenazine-2,3-diol and phenazinone derivatives in solvent at room temperature (298 K) exhibit fluorescence emission properties with the τ_{fl} values in the order of ns.

^{1}H NMR spectral measurements

In order to determine the chemical species of **PD1** and **PD2** in solvent, we performed ^{1}H NMR spectral measurements on **PD1** and **PD2** in THF-d_8 with and without the addition of deuterated water (D_2O), in comparison with those on **PZ1** and **PZ2** (Fig. 6 and S9–S14†). The ^{1}H NMR spectra of **PD1** in THF-d_8 both with and without the addition of D_2O are broadened (Fig. 6a). On the other hand, the ^{1}H NMR spectra of **PD2** show sharp signals in THF-d_8 without D_2O, but they become broad

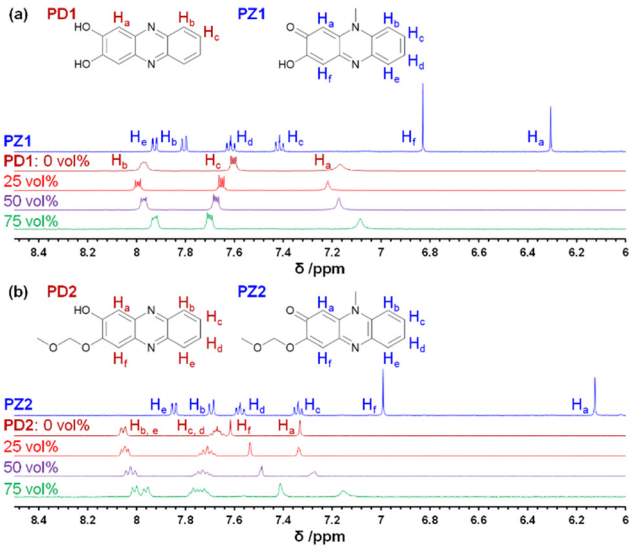

Fig. 6 ^{1}H NMR spectra of (a) **PD1** in THF-d_8 without D_2O and with 25–75 vol% D_2O content and **PZ1** in THF-d_8 and (b) **PD2** in THF-d_8 without D_2O and with 25–75 vol% D_2O content and **PZ2** in THF-d_8.

signals upon the addition of D_2O to the THF-d_8 solution (Fig. 6b). Meanwhile, the ^{1}H NMR spectra of **PD1** and **PD2** are totally different from those of **PZ1** and **PZ2** which show sharp signals: the chemical shifts (δ) of the proton (H_a) adjacent to the hydroxy group at 7.1–7.3 ppm and the proton (H_f) adjacent to the methoxymethoxy group at 7.4–7.6 ppm for **PD1** and **PD2** show a considerable downfield shift, compared to the corresponding ones (the α-proton (H_a) of the carbonyl moiety at 6.1–6.3 ppm and the proton (H_f) adjacent to the hydroxy group at 6.8–7.0 ppm) for **PZ1** and **PZ2**. Moreover, it is worth mentioning here that for **PD1** and **PD2**, the ratio of the integrated signal of H_a decreases with an increase in D_2O content in the THF-d_8 solution (the integrated intensity of H_a = 1, 0.84, 0.82, and 0.78 for 0, 25, 50 and 75 vol% water content, respectively), indicating hydrogen/deuterium exchange (H/D exchange) between D_2O and the enolate ion **Keto 1** in a resonance hybrid, as shown in Scheme 3, that is, phenoxide ions (**PD1-P** and **PD2-P**), **Keto 1** and the phenazinone structure **Keto 2** are present as keto–enol anion resonance structures formed through the enol–enolate ion equilibrium. The fact indicates that not only do **PD1** and **PD2** exist mainly as the phenoxide

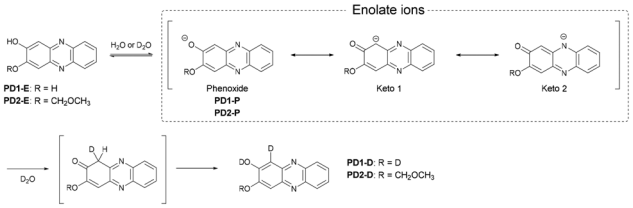

Scheme 3 Proposed mechanism for the formation of deuterated **PD1-D** and **PD2-D** by hydrogen/deuterium exchange through the enol–enolate ion equilibrium.

ion and the diol or mono-ol structure through the enol–enolate ion equilibrium between them, respectively, but also **Keto 2** is the most minor contributor in the resonance hybrid and thus the formation of the phenazinone structure is negligible in the solutions. Not surprisingly, such H/D exchange was not observed in the case of **PD3** (Fig. S14†).

ESInterPT and photochromic properties

In order to investigate the ESInterPT and photochromic properties of phenazine-2,3-diol (**PD1**) and its alkoxy derivatives (**PD2** and **PD3**), we conducted photoabsorption and photoluminescence spectral measurements of **PD1–3**, **PZ1**, and **PZ2** in 2-MeTHF at room temperature (298 K) and in a glassy matrix of 2-MeTHF at 77 K (Fig. 7) before and after photoirradiation with monochromic light at 385 nm. The photoabsorption and photoluminescence spectral properties of **PD1–3**, **PZ1**, and **PZ2** in 2-MeTHF at 298 K were similar to those in THF at 298 K (Fig. 3 and 7). Meanwhile, the photoabsorption spectra of **PD1–3**, **PZ1**, and **PZ2** at 77 K were similar to those at 298 K, but they exhibited a vibronically-structured photoabsorption band (Fig. 7a, c, e, g, and i). Interestingly, for **PD1**, the broad photoabsorption band at 480 nm disappeared at 77 K (Fig. 7a), indicating a complete shift in the enol–enolate ion equilibrium from the enolate ion form (**PD1-P**) to the enol form (**PD1-E**) (Scheme 3). It is worth noting here that upon photoirradiation (λ = 385 nm) at 77 K, the photoabsorption spectra of **PD1** and **PD2** exhibited new vibronically-structured photoabsorption bands in the range of 400 nm–550 nm (Fig. 7a and c) which are similar to those of **PZ1** and **PZ2**, whereas the photoabsorption spectra of **PD3**, **PZ1**, and **PZ2** did not undergo appreciable changes in the absorbance and shape (Fig. 7e, g, and i). This result indicates the formation of keto forms **PD1-K** and **PD2-K** upon photoirradiation at 77 K, that is, the photochromism of **PD1** and **PD2** through the ESInterPT processes based on keto–enol tautomerization from **PD1-E** and **PD2-E** to **PD1-K** and **PD2-K**, respectively (Fig. 2). Actually, upon photoirradiation (λ = 385 nm) at 77 K, the colorless solutions of **PD1** and **PD2** transformed into orange-colored solutions (Fig. 8a–f), which are similar in color to the solutions of **PZ1** and **PZ2** (Fig. S41 and S42†). When the orange-colored solutions were left to stand at room temperature, they recovered to their original colorless form. On the other hand, **PD3** solution remained colorless even after photoirradiation (λ = 385 nm) at 77 K (Fig. 8g–i).

The photoluminescence spectral measurement before and after photoirradiation at 77 K provided conclusive evidence for the formation of keto forms of **PD1** and **PD2** based on keto–enol tautomerization. Indeed, in the corresponding photoluminescence spectra of **PD1** and **PD2**, new vibronically-structured photoluminescence bands appeared in the range of 500–750 nm after photoirradiation (λ = 385 nm) at 77 K, although they are also observed before photoirradiation (λ = 385 nm) because of the photoabsorption bands at 400–550 nm (Fig. 7a and c) which emerged upon photoexcitation (λ^{ex} = 400 nm for **PD1** and 395 nm for **PD2**) during the photoluminescence spectral measurement. For **PD3** at 77 K, a new

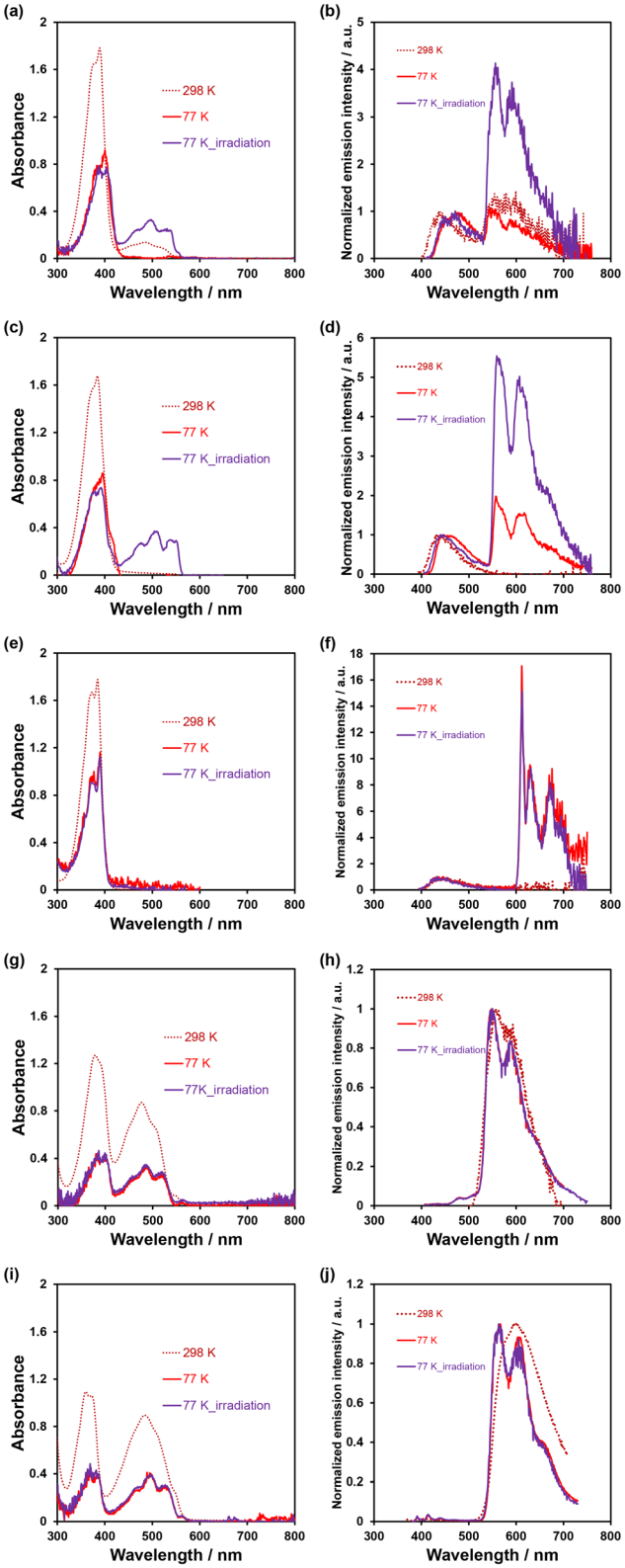

Fig. 7 Photoabsorption and photoluminescence spectra of (a and b) **PD1** (λ^{ex} = 389–400 nm), (c and d) **PD2** (λ^{ex} = 384–395 nm), (e and f) **PD3** (λ^{ex} = 385 nm), (g and h) **PZ1** (λ^{ex} = 379–386 nm), and (i and j) **PZ2** (λ^{ex} = 372–383 nm) in 2-MeTHF (1.0×10^{-4} M) at 298 K (dashed line) and 77 K (solid line) before and after irradiation with monochromic light at 385 nm.

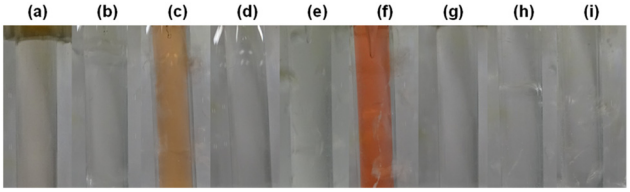

Fig. 8 Photographs of (a)–(c) **PD1** (a: 298 K, b: 77 K, and c: 77 K after photoirradiation at 385 nm), (d)–(f) **PD2** (d: 298 K, e: 77 K, and f: 77 K after photoirradiation at 385 nm), and (g)–(i) **PD3** (g: 298 K, h: 77 K, and i: 77 K after photoirradiation at 385 nm) in 2-MeTHF.

vibronically-structured photoluminescence band appeared in the range of 600–750 nm, but the photoluminescence band remained constant in intensity and shape even after photoirradiation (λ = 385 nm). On the other hand, the photoluminescence spectra of **PZ1** and **PZ2** at 77 K exhibited vibronically-structured photoluminescence bands in the range of 500–750 nm (Fig. 7h and j), but they are similar in intensity and shape before and after photoirradiation (λ = 385 nm) at 77 K. Furthermore, in order to assign the origins of photoluminescence bands of **PD1–3**, **PZ1**, and **PZ2** at 77 K, we performed phosphorescence spectral measurements with an initial delay of 100 μs and time resolved phosphorescence decay analysis (Fig. S43–S46†). For **PD3** at 77 K, a phosphorescence band with a long lifetime (τ_{pl} = 37.3 ms, Fig. S43 and S44†) was observed in the range of 600–750 nm which is similar to the photoluminescence spectrum without initial delay (Fig. 7f). Obviously, the fact reveals that for **PD3** at 77 K, the vibronically-structured photoluminescence band at 600–750 nm could be assigned to the phosphorescence emission originating from the phenazine skeleton. However, for **PZ1** and **PZ2** before and after photoirradiation (λ = 385 nm) at 77 K, the phosphorescence spectrum was not observed, thus the photoluminescence bands at 500–750 nm are assigned to the fluorescence emission originating from the phenazinone skeleton, as in the case of 298 K. On the other hand, **PD1** and **PD2** before and after photoirradiation (λ = 385 nm) at 77 K exhibited phosphorescence bands with long lifetimes (τ_{pl} = 28.6 ms for **PD1** and 32.0 ms for **PD2**) in the range of 600–750 nm which are different in the range of emission wavelengths from the photoluminescence spectrum (500–750 nm) without initial delay (Fig. 7b and d) but are similar in that to the photoluminescence (phosphorescence) spectrum (600–750 nm) of **PD3** at 77 K (Fig. 7f). These observations indicate that for the photoluminescence characteristics of **PD1** and **PD2** upon photoirradiation (λ = 385 nm) at 77 K, the photoluminescence bands at 500–750 nm are assigned to the fluorescence emission originating from the partially formed **PD1-K** and **PD2-K**, and the photoluminescence bands at 600–750 nm are assigned to the phosphorescence emission originating from the residual **PD1-E** and **PD2-E**, whereas the photoluminescence bands before photoirradiation (λ = 385 nm) at 77 K are mainly due to the phosphorescence emission originating from **PD1-E** and **PD2-E**. Therefore, this result strongly supports the photochromism of **PD1** and **PD2** through the ESInterPT processes based on keto–enol tautomerization in the glassy matrix at 77 K. Furthermore, the appearance of photoabsorption bands originating from the keto forms **PD1-K** and **PD2-K** upon photoirradiation (λ = 385 nm) at 77 K was observed even in a low-concentration solution of 10 μM (Fig. S40†). The fact indicates that an aggregate of the enol form (**PD1-E** and **PD2-E**) is formed through the intermolecular hydrogen bonding in the glassy matrix at a low temperature, and then ESInterPT proceeds rapidly because in the excited state, the keto form becomes more stable than the enol form, as reported by Ogawa *et al.*[15]

Single crystal X-ray structural analysis

One would make the assumption that the ESInterPT process requires the presence of intermolecular hydrogen bonding between proton donors and acceptors. Thus, to investigate the formation of the hydrogen bonding for **PD1** and **PD2** in the aggregate state, single-crystal X-ray structural analyses for **PD1** and **PD2** were performed, in comparison with those for **PZ1** and **PZ2** in our previous study[17] (Fig. 9 and 10). Surprisingly, this report is the first to achieve the crystal structural analyses of phenazine-2,3-diol **PD1** and its monoalkoxy derivative **PD2**, although the synthesis of **PD1** was reported 70 years ago[19a] and its characterization was fully determined by NMR spectral analysis 15 years ago.[19b] A crystal of **PD1** was obtained by sublimation of a powdery solid, because recrystallization from solution provided the powdery solid. Meanwhile, a crystal of **PD2** was prepared by recrystallization from an ethanol solution. It is worth mentioning here that the **PD1** molecule exists in the keto form (**PD1-K**) in the crystal, but the **PD2** molecule exists in the enol form (**PD2-E**) in the crystal (Fig. 9a and b), although the crystal structure of **PD2-E** has two crystallographically independent molecules in which each molecule has slightly different bond lengths and angles (Fig. S3†). Actually, for **PD1**,

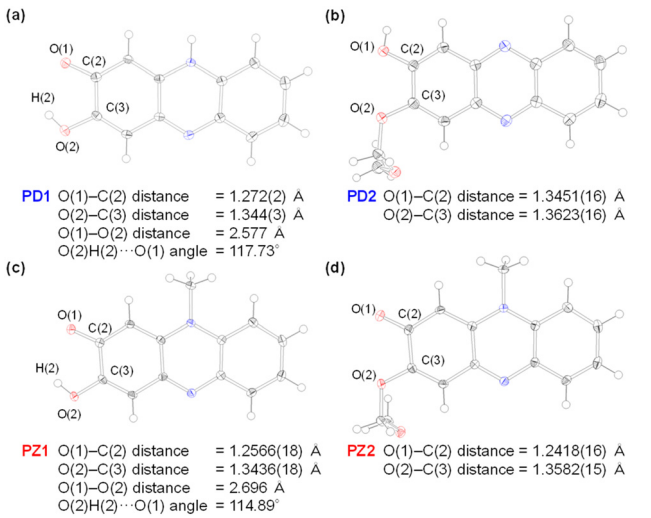

Fig. 9 X-ray crystal structures of (a) **PD1**, (b) **PD2**, (c) **PZ1**, and (d) **PZ2** measured at 100 K. Ellipsoids are shown at the 50% probability level.

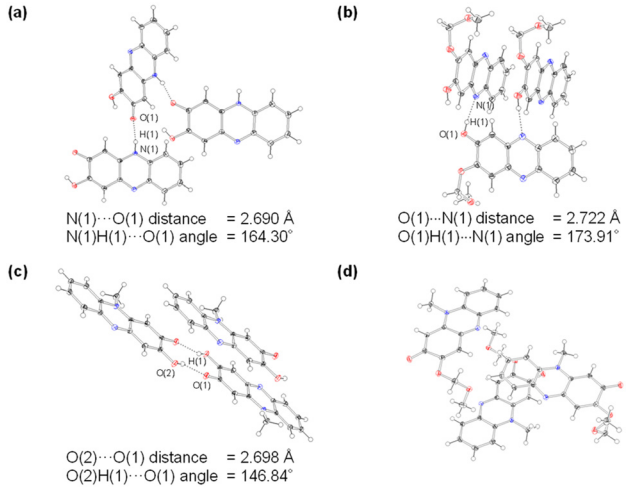

Fig. 10 Crystal packing structures of (a) **PD1**, (b) **PD2**, (c) **PZ1**, and (d) **PZ2** measured at 100 K. The hydrogen bonds are indicated by dotted lines. Ellipsoids are shown at the 50% probability level.

the observed O(1)–C(2) and O(2)C(3) bond lengths are 1.272(2) Å and 1.344(3) Å, respectively, which are typical C═O double bond and C–O single bond lengths, respectively.[21] Indeed, the C═O double bond and C–O single bond lengths of **PD1-K** are similar to those (1.2566(18) Å and 1.2418(16) Å for O(1)–C(2) bond length and 1.3436(18) Å and 1.3582(15) Å for O(2)–C(3) bond length, respectively) of **PZ1** and **PZ2** (Fig. 9c and d). On the other hand, for **PD2-E**, the observed bond lengths of O(1)–C(2) and O(2)–C(3) are 1.3451(16) Å and 1.3623(16) Å, respectively, indicating C–O single bond lengths. Thus, our work first verified the existence of keto and enol forms for phenazine2,3-diol and its alkoxy derivative by single-crystal X-ray structural analyses. Furthermore, it was found that the **PD1-K** molecule is in the *syn*-conformation where the hydrogen atom of the hydroxy group is directed toward the oxygen atom of the carbonyl group, indicating the formation of intramolecular hydrogen bonding between them (O(2)H(2)···O(1) angle = *ca.* 117.73° and O(1)···O(2) distance = 2.577 Å), as in the case of **PZ1** (O(2)H(2)···O(1) angle = *ca.* 114.89° and O(1)···O(2) distance = 2.696 Å). Meanwhile, the **PD2-E** molecule is in the *anti*-conformation where the hydrogen atom of the hydroxy group faces in the direction opposite to the oxygen atom of the methoxymethoxy group, indicating a lack of intramolecular hydrogen bonding between them. As a result, *syn*-**PD1-K** molecules form the intermolecular NH···O hydrogen bonding with N(1)H(1)···O(1) angle = *ca.* 164° and N(1)···O(1) distance = 2.690 Å between the hydrogen atom of the amino moiety and the oxygen atom of the carbonyl group (Fig. 10a). On the other hand, *anti*-**PD2-E** molecules form the intermolecular OH···N hydrogen bonding with O(1)H(1)···N(1) angle = *ca.* 174° and O(1)···N(1) distance = 2.722 Å between the hydrogen atom of the hydroxy group and the nitrogen atom of the phenazine skeleton (Fig. 10b). Hence, neighboring *syn*-**PD1-K** and *anti*-**PD2-E** molecules are linked by the intermolecular NH···O hydrogen bonding and OH···N hydrogen bonding, respectively, to form one-dimensional molecular chains. Meanwhile, **PZ1** molecules form a dimer by the intermolecular OH···O hydrogen bonding with O(2)H(2)···O(1) angle = *ca.* 147° and O(2)···O(1) distance = 2.698 Å between the hydrogen atom of the hydroxy group and the oxygen atom of the carbonyl group (Fig. 10c). Of course, such intramolecular and intermolecular hydrogen bonding were not observed in the crystal of **PZ2** (Fig. 10d). Thus, the fact suggests strongly that for **PD1** and **PD2**, the formation of continuous intermolecular hydrogen bonding in the aggregate is involved in the keto–enol tautomerization of phenazine-2,3-diol derivatives based on ESInterPT.

Solid-state optical properties

In order to explore the expression of chromism based on the keto–enol tautomerization of **PD1–3** in the solid state, we performed UV-vis diffuse reflectance-absorption and fluorescence spectral measurements of the solids before and after photoirradiation (λ = 385 nm) at 298 K and 77 K and differential scanning calorimetry (DSC) of the solids after heating and cooling. The colors at 298 K were dark red for **PD1-K**, yellow for **PD2-E**, and white for **PD3** (Fig. 11a, e, and i). Thus, the color of **PD1-K** is similar to those of **PZ1** and **PZ2** which is attributed to the formation of the keto form in the crystal (Fig. 11m and n). Indeed, the photoabsorption band of **PD1-K** in the solid state is significantly broadened in a longer wavelength region with an onset of *ca.* 650 nm (Fig. 12a) compared with those in THF

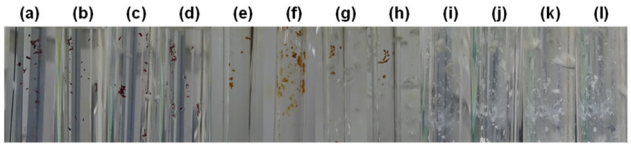

Fig. 11 Photographs of (a)–(d) **PD1-K** (a: 298 K, b: 298 K after photoirradiation at 385 nm, c: 77 K, and d: 77 K after photoirradiation at 385 nm), (e)–(h) **PD2-E** (e: 298 K, f: 298 K after photoirradiation at 385 nm, g: 77 K, and h: 77 K after photoirradiation at 385 nm), and (i)–(l) **PD3** (i: 298 K, j: 298 K after photoirradiation at 385 nm, k: 77 K, and l: 77 K after photoirradiation at 385 nm).

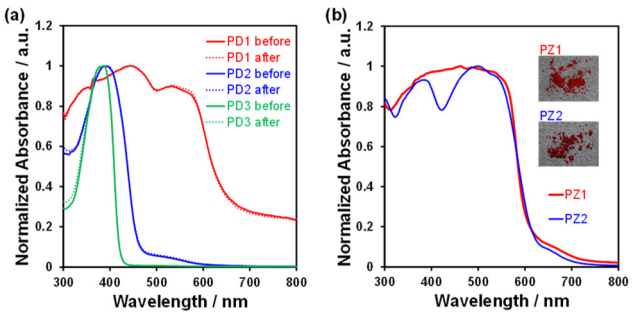

Fig. 12 Solid-state UV-vis diffuse reflectance-absorption spectra of (a) **PD1–3** before and after irradiation with monochromic light at 385 nm at 298 K and (b) **PZ1** and **PZ2**. Insets in (b): photographs of the solids of **PZ1** and **PZ2**.

(Fig. 3a), but it is similar to those of **PZ1** and **PZ2** in the solid state (Fig. 12b). On the other hand, the photoabsorption maximum wavelengths ($\lambda_{max}^{abs-solid}$) of **PD2-E** and **PD3** in the solid state appeared at around 385 nm, which are similar to those in THF (Fig. 3a). It was found that for **PD1–3**, there were no changes in their colors and photoabsorption spectra before and after photoirradiation (λ = 385 nm) at 298 K and 77 K (Fig. 11b–d, f–h, j–i, and 12a), although we could not obtain the photoabsorption spectra at 77 K due to technical difficulties. Meanwhile, the precise observation of fluorescence spectra for **PD1–3**, **PZ1**, and **PZ2** in the solid state was difficult due to their feeble solid-state fluorescence properties.

The DSC analysis of **PD1–3** provided a valuable insight into the chromism of phenazine-2,3-diol derivatives based on the keto–enol tautomerization (Fig. 13a). The DSC curves of **PD1–3** showed that in the cooling process from 25 °C to −80 °C, there is no observable peak for the DSC traces. In the heating process from 25 °C to 250 °C, the DSC trace of **PD1-K** has no observable peak; meanwhile, the DSC trace of **PD3** has only one sharp endothermic melting (T_m) peak at 137 °C. On the other hand, the DSC trace of **PD2-E** shows an endothermic peak associated with sublimation (T_s) at 181 °C, and then an exothermic oxidative decomposition (T_d)[22] at 188 °C which is also supported by thermogravimetry and differential thermal analysis (TG-DTA) (Fig. 13b and S56†). Interestingly, for **PD2**, a wire-like solid was obtained as the sublimate (Fig. 14d and e)

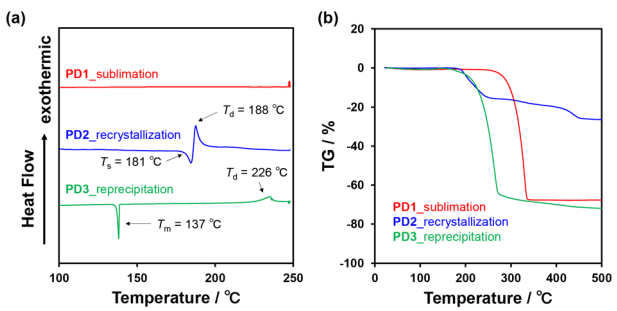

Fig. 13 (a) DSC curves (heating process from 25 °C to 250 °C at a scan rate of 1 °C min^{-1}) and (b) TG curves (heating process from 25 °C to 500 °C at a scan rate of 10 °C min^{-1}) of **PD1–3**.

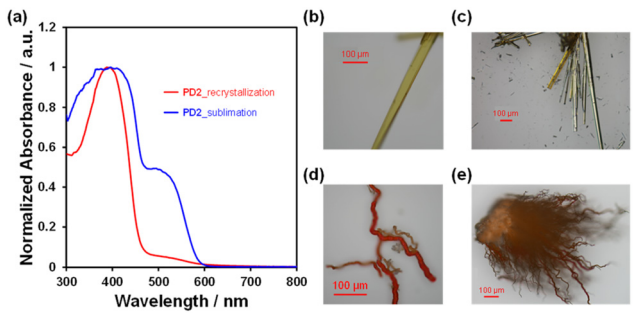

Fig. 14 (a) Solid-state UV-vis diffuse reflectance-absorption spectra of the crystals of **PD2** and the solids of the sublimate obtained by heating the crystals of **PD2** at 133 °C under vacuum. Photographs of (b and c) the crystals and (d and e) the solids of the sublimate for **PD2**.

by heating the needle-like crystal (Fig. 14b and c) of **PD2-E** at 133 °C under vacuum. The wire-like solid of the sublimate for **PD2** shows a red color and a broad photoabsorption band in a longer wavelength region with an onset of *ca.* 600 nm (Fig. 14a), which are similar to the colors and the photoabsorption spectra of the crystals of **PD1-K** as well as **PZ1** and **PZ2** (Fig. 12); meanwhile, for the solid of the sublimate, the ^{1}H NMR spectrum in DMSO-d_6 was assigned to the enol form of **PD2** and the HRMS analysis demonstrated the presence of a **PD2** base peak (Fig. S57, S62, and S63†). Furthermore, the solids of the sublimate for **PD2** have a different DSC trace and X-ray powder diffraction (XRD) pattern from the crystals of **PD2-E**; the sublimate of **PD2** showed T_s at 169 °C and then T_d at 181 °C and different diffraction peaks in the range of 2θ = 20–30° from the crystals of **PD2-E** (Fig. S58 and S59†). Thus, this result suggests that the **PD2** molecule exists in the keto form (**PD2-K**) in the solid of the sublimate, while unfortunately, we could not perform X-ray structural analysis due to an insufficient size of the wire-like solid (Fig. 14d, and e) and it was also difficult to characterize the sublimate as **PD2-K** by FT-IR spectral analysis (Fig. S49†). It is worth mentioning again that the needle-like crystal of **PD1**, which was obtained by sublimation of the powdery solid, is composed of the **PD1-K** molecule in the keto form (Fig. 9a and 10a). Meanwhile, for the keto–enol tautomerization in the solid state, Ogawa *et al.* have reported that salicylideneanilines show solid-state thermochromism which is ascribed to the tautomeric equilibrium between the enol and *cis*-keto forms; the *cis*-keto form exists in the crystal at 298 K, but at a low temperature (77 K), the *cis*-keto form shows a decrease in pollution due to the formation of the enol form.[23] Thus, although **PD1** and **PD2** did not show thermochromism as well as photochromism in the crystalline state, we believe that this interesting result provides a valuable insight for a greater understanding of the keto–enol tautomerization of phenazine-2,3-diol derivatives and their photophysical properties in the solution and in the solid state.

Theoretical calculations

The thermodynamic stabilities of **PD1-E**, **PD1-K**, **PD2-E**, and **PD2-K** were estimated using density functional theory (DFT) calculations at the B3LYP/6-311G(d,p) level,[24] where for the convenience of calculations, the methoxymethoxy group of **PD2-E** and **PD2-K** was replaced with the methoxy group (Fig. 15). In order to compare with the conformers *syn*-**PD1-K** and *anti*-**PD2-E** in the crystals, we included the conformers for **PD1-E**, **PD1-K**, and **PD2-E** in the DFT calculations; for the enol form **PD1-E**, *anti*-**PD1-E** and *syn*-**PD1-E** are in the *anti*-conformation and *syn*-conformation, respectively, where the two hydrogen atoms of hydroxy groups face in the opposite directions for the former but in the same direction for the latter. For the keto form **PD1-K**, *anti*-**PD1-K** and *syn*-**PD1-K** are in the *anti*-conformation and *syn*-conformation, respectively, that is, the hydrogen atom of the hydroxy group faces in the direction opposite to the oxygen atom of the carbonyl group for the former but is directed toward that for the latter. On the other hand, for the enol form **PD2-E**, *anti*-**PD2-E** and *syn*-**PD2-E** are

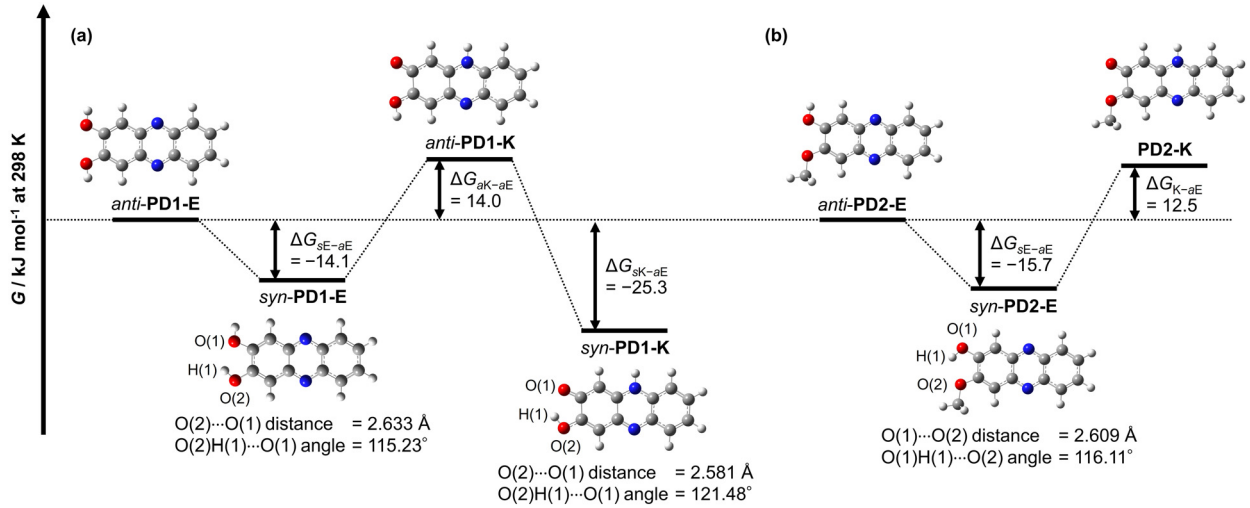

Fig. 15 Gibbs free energy diagram for optimized geometries of conformers and tautomers for (a) **PD1** and (b) **PD2** estimated using DFT calculations at the B3LYP/6-311G(d,p) level. The Gibbs free energies for *anti*-**PD1-E** and *anti*-**PD2-E** are set as zero in each category to estimate the difference (ΔG) in G between *anti*-**PD1-E** or *anti*-**PD2-E** and the other conformer or the tautomer. For convenience of calculations, the methoxymethoxy groups of *anti*-**PD2-E**, *syn*-**PD2-E**, and **PD2-K** were replaced with the methoxy groups.

in the *anti*-conformation and *syn*-conformation, respectively, where the hydrogen atom of the hydroxy group faces in the direction opposite to the oxygen atom of the methoxy group for the former but is directed toward that for the latter. Based on the optimized geometries, understandably, there is no formation of intramolecular hydrogen bonding between the two hydroxy groups, the hydroxy group and the carbonyl group, or the hydroxy group and the methoxy group for *anti*-**PD1-E**, *anti*-**PD1-K**, *anti*-**PD2-E**, as well as **PD2-K**. On the other hand, the angles of O(2)H(1)···O(1) for *syn*-**PD1-E** and *syn*-**PD1-K** and O(2)H(1)···O(1) for *syn*-**PD2-E**, which involve the formation of intramolecular hydrogen bonding, are *ca.* 115°, *ca.* 121°, and *ca.* 116°, respectively. The fact indicates the existence of intramolecular hydrogen bonding between the two hydroxy groups for *syn*-**PD1-E**, and the hydroxy group and the carbonyl group for *syn*-**PD1-K**, and the hydroxy group and the methoxy group for *syn*-**PD2-E**.

Meanwhile, the Gibbs free energies (G) for *anti*-**PD1-E** and *anti*-**PD2-E** are set as zero in each category to estimate the difference (ΔG) in the G between *anti*-**PD1-E** or *anti*-**PD2-E** and the other conformer or the tautomer (Fig. 15). The obtained ΔG values of *syn*-**PD1-E**, *anti*-**PD1-K**, and *syn*-**PD1-K** were estimated to be −14.1 kJ mol^{-1}, 14.0 kJ mol^{-1}, and −25.3 kJ mol^{-1}, respectively (Fig. 15a). This result indicates that *syn*-**PD1-E** and *syn*-**PD1-K** are thermodynamically stabilized by the formation of intramolecular hydrogen bonding, compared to *anti*-**PD1-E** and *anti*-**PD1-K**. Thus, this result reveals that of the conformers and the tautomers of **PD1**, *syn*-**PD1-K**, which exists in the crystal (Fig. 9a and 10a), is thermodynamically the most stable. For **PD2**, on the other hand, the obtained ΔG values showed that the enol forms *anti*-**PD2-E** and *syn*-**PD2-E** are thermodynamically more stable than the keto form **PD2-K**, and also indicated that *anti*-**PD2-E**, which exists in the crystal, is thermodynamically less stable than *syn*-**PD2-E** with a ΔG value of −15.7 kJ mol^{-1} which is stabilized by the formation of the intermolecular hydrogen bonding (Fig. 15b). Thus, based on this result, it is suggested that the formation of one-dimensional intermolecular hydrogen bonding by the most stable tautomer *syn*-**PD1-K** constructs a thermodynamically stable crystal structure. For **PD2**, *anti*-**PD2-E** can form intermolecular hydrogen bonding because the hydrogen atom of the hydroxy group faces in the direction opposite to the oxygen atom of the methoxy group, but it is difficult for *syn*-**PD2-E** to form intermolecular hydrogen bonding due to its structure with intramolecular hydrogen bonding. Consequently, it was suggested that the crystal structure constructed by *anti*-**PD2-E** is thermodynamically stabilized by the formation of one-dimensional intermolecular hydrogen bonding (Fig. 9b and 10b), although *anti*-**PD2-E** is thermodynamically less stable than *syn*-**PD2-E**.

To further understand the optical properties of phenazine-2,3-diol derivatives, time-dependent DFT (TDDFT) calculations were performed for the conformers and the tautomers **PD1-E**, **PD1-K**, **PD2-E**, and **PD2-K** and **PD3** (Fig. 16, Fig. S26 and Table S13†). All the enol tautomers, *anti*-**PD1-E**, *syn*-**PD1-E**, *anti*-**PD2-E**, and *syn*-**PD2-E**, and **PD3** showed $S_0 \rightarrow S_3$ ($\pi\pi^*$) transitions at around 360 nm with oscillator strengths (f) = 0.25–0.30 (Fig. 16b and f, *e.g.*, *syn*-**PD1-E** and *syn*-**PD2-E**), which are mainly attributed to the transitions (*ca.* 85%) from the HOMO−1 to the LUMO, where both the HOMO−1 and LUMO are delocalized over the phenazine skeleton including the hydroxy and the methoxy group. On the other hand, for the keto tautomers, the differences in transition characteristics were observed depending on the direction (*anti*- or *syn*-) of the hydrogen atom of the hydroxy group. All the keto tautomers, *anti*-**PD1-K**, *syn*-**PD1-K**, and **PD2-K**, showed $S_0 \rightarrow S_1$ ($\pi\pi^*$) transitions at around 440 nm with the oscillator strengths (f) of

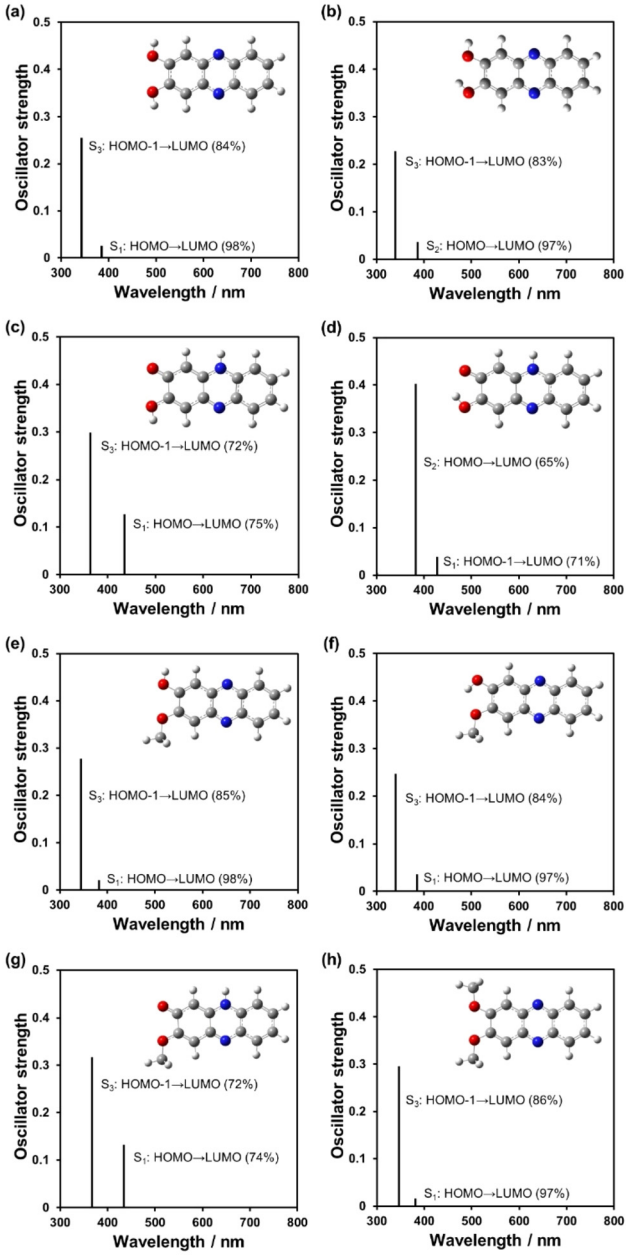

Fig. 16 Calculated photoabsorption spectra of (a) *anti*-**PD1-E**, (b) *syn*-**PD1-E**, (c) *anti*-**PD1-K**, (d) *syn*-**PD1-K**, (e) *anti*-**PD2-E**, (f) *syn*-**PD2-E**, (g) **PD2-K**, and (h) **PD3** derived from TDDFT calculations at the B3LYP/6-311G(d,p) level. For convenience of calculations, the methoxymethoxy groups of *anti*-**PD2-E**, *syn*-**PD2-E**, **PD2-K**, and **PD3** were replaced with the methoxy groups.

0.13 for *anti*-**PD1-K** and **PD2-K**, and 0.039 for *syn*-**PD1-K**, which are mainly attributed to the transitions from the HOMO to the LUMO for *anti*-**PD1-K** and **PD2-K** (*ca.* 75%), and the transition from the HOMO–1 to the LUMO for *syn*-**PD1-K** (71%). Both the HOMO and LUMO of *anti*-**PD1-K**, *syn*-**PD1-K**, and **PD2-K** are delocalized over the phenazinone skeleton including the hydroxy group or/and the methoxy group, and the HOMO–1 of *syn*-**PD1-K** is delocalized on the partial phenazinone skeleton and the hydroxy group, excluding the carbonyl moiety. Moreover, these keto tautomers showed $S_0 \rightarrow S_3$ ($\pi\pi^*$) transitions at around 360 nm with oscillator strengths (f) = 0.30–0.32 for *anti*-**PD1-K** and **PD2-K**, and the $S_0 \rightarrow S_2$ ($\pi\pi^*$) transitions at around 380 nm with the oscillator strength (f) = 0.40 for *syn*-**PD1-K**, which are mainly attributed to the transitions from the HOMO–1 to the LUMO (72%) for *anti*-**PD1-K** and **PD2-K**, and the transition from the HOMO to the LUMO for *syn*-**PD1-K** (65%). Such transition characteristics were also observed between *anti*-**PZ1** and *syn*-**PZ1** (Fig. S23, S24, and S25†). Consequently, the TDDFT calculations revealed that for **PD1** and **PD2**, the keto forms show photoabsorption bands in a longer wavelength region, compared to the enol forms, and thus are in good agreement with the photoabsorption spectra of **PD1**, **PD2**, and **PD3** in 2-MeTHF, indicating the existence of the enol form at 298 K and the existence of the keto form in a glassy matrix at 77 K (Fig. 7a, c, and e). Therefore, our work first verified that phenaznine-2,3-diol and its monoalkoxy derivative exhibit photochromism through the ESInterPT processes based on keto–enol tautomerization.

Conclusions

In this study, we verified that phenazine-2,3-diol **PD1** and its monoalkoxy derivative **PD2** exhibit photochromism through the ESInterPT processes based on keto–enol tautomerization in a glassy matrix at 77 K. Indeed, it was found that the colorless solutions of enol forms **PD1-E** and **PD2-E** at 298 K and 77 K transformed into orange-colored solutions of keto forms **PD1-K** and **PD2-K** upon photoirradiation (λ = 385 nm) at 77 K. In a glassy matrix at 77 K, **PD1** and **PD2** exhibit phosphorescence emission originating from the enol forms before photoirradiation but exhibit fluorescence emission originating from the keto forms after photoirradiation, confirming the ESInterPT processes based on keto–enol tautomerization. Furthermore, it is worth mentioning that **PD1** and **PD2** molecules exist in the keto form (**PD1-K**) and the enol form (**PD2-E**) that construct the one-dimensional intermolecular NH···O hydrogen bonding and OH···N hydrogen bonding, respectively, in the crystal. More interestingly, based on the photoabsorption spectrum, the DSC trace, and the XRD pattern of the solid obtained by sublimation of the crystals of **PD2-E**, it was suggested that the **PD2** molecule exists in the keto form (**PD2-K**) in the solid of the sublimate. The facts indicate strongly that for **PD1** and **PD2**, the formation of continuous intermolecular hydrogen bonding in aggregates such as in a glassy matrix at 77 K is involved in the keto–enol tautomerization of phenazine-2,3-diol derivatives based on ESInterPT. Therefore, this study not only provides a valuable insight for a greater understanding of ESInterPT based on the keto–enol tautomerization of phenazine-2,3-diol derivatives but also offers an important insight into the photochromism of diazaacene-diols such as diaza-naphthalene and diaza-anthracence derivatives with two hydroxy groups. Indeed, the investigation of the expression of thermochromism as well as photochro-

mism of phenazine-2,3-diol derivatives in the solid state is ongoing in our laboratory.

Data availability

The full experimental details, synthetic procedures, characterization data, the ^{1}H, ^{13}C-NMR, FT-IR, and HRMS spectra of products, single-crystal X-ray structural analyses, differential scanning calorimetry (DSC), thermogravimetry (TG) and differential thermal analysis (TG-DTA), photoabsorption and fluorescence spectra, computational details, and supplementary discussions associated with this article are provided in the ESI.†

Author contributions

Y.O. conceived the project and directed the experimental studies. K. O. performed almost all the experiments and carried out DFT calculations. K. K. and M. Y. helped with synthesis and purification of compounds. N. K. helped with differential scanning calorimetry (DSC), thermogravimetry (TG) and differential thermal analysis (TG-DTA). K. I. conducted photoabsorption and fluorescence spectral measurements at 77 K. The manuscript was written through contributions of all authors.

Conflicts of interest

There are no conflicts to declare.

Acknowledgements

This work was supported by Grants-in-Aid for Scientific Research (B) from the Japan Society for the Promotion of Science (JSPS) KAKENHI Grant Number 22H02123 and by the Yashima Environment Technology Foundation. K. O. was supported by JST, the Establishment of University Fellowships towards the Creation of Science Technology Innovation, Grant Number JPMJF2129.

References

1 (*a*) J. Zhao, S. Ji, Y. Chen, H. Guo and P. Yang, *Phys. Chem. Chem. Phys.*, 2012, **14**, 8803–8817; (*b*) J. Piechowska, K. Virkki, B. Sadowski, H. Lemmetyinen, N. V. Tkachenko and D. T. Gryko, *J. Phys. Chem. A*, 2014, **118**, 144–151; (*c*) M. R. Aronoff, B. VanVeller and R. T. Raines, *Org. Lett.*, 2013, **15**, 5382–5385; (*d*) M. Takahashi, K. Sakai, K. Sambe and T. Akutagawa, *J. Phys. Chem. B*, 2022, **126**, 3116–3124; (*e*) K. Sakai, N. Miyamoto, M. Ogawa, K. Kawano and T. Akutagawa, *J. Phys. Chem. A*, 2021, **125**, 4784–4792; (*f*) A. Bhattacharyya, S. C. Makhal and N. Guchhait, *Chem. Phys.*, 2019, **520**, 61–69; (*g*) P. Jurek, H. Jędrzejewska, M. F. Rode and A. Szumna, *Chem. – Eur. J.*, 2022, **29**, e202203116; (*h*) T. Mutai, H. Sawatani, T. Shida, H. Shono and K. Araki, *J. Org. Chem.*, 2013, **78**, 2482–2489; (*i*) J. Massue, D. Jacquemin and G. Ulrich, *Chem. Lett.*, 2018, **47**, 1083–1089; (*j*) D. Göbel, D. Duvinage, T. Stauch and B. J. Nachtsheim, *J. Mater. Chem. C*, 2020, **8**, 9213–9225.

2 (*a*) Y. Zhang, H. Yang, H. Ma, G. Bian, Q. Zang, J. Sun, C. Zhang, Z. An and W.-Y. Wong, *Angew. Chem., Int. Ed.*, 2019, **58**, 8773–8778; (*b*) I. Allison, M. Mamada, A. Shukla, S. K. M. McGregor, R. B. Roseli, I. Gale, V. P. Rahane, E. G. Moore, E. H. Krenske, N. Jain, C. Adachi, E. B. Namdas and S.-C. Lo, *J. Mater. Chem. C*, 2023, **11**, 15861–15872.

3 (*a*) S.-H. Hwang, H. Kim, H. Ryu, I. Serdiuk, D. Lee and T.-L. Choi, *J. Am. Chem. Soc.*, 2022, **144**, 1778–1785; (*b*) K. Sakai, T. Ishikawa and T. Akutagawa, *J. Mater. Chem. C*, 2013, **1**, 7866–7871.

4 (*a*) S. Hayashi, E. Tajkhorshid and K. Schulten, *Biophys. J.*, 2002, **83**, 1281–1297; (*b*) E. Nango, A. Royant, M. Kubo, T. Nakane, C. Wickstrand, T. Kimura, T. Tanaka, K. Tono, C. Song, R. Tanaka, T. Arima, A. Yamashita, J. Kobayashi, T. Hosaka, E. Mizohata, P. Nogly, M. Sugahara, D. Nam, T. Nomura, T. Shimamura, D. Im, T. Fujiwara, Y. Yamanaka, B. Jeon, T. Nishizawa, K. Oda, M. Fukuda, R. Andersson, P. Båth, R. Dods, J. Davidsson, S. Matsuoka, S. Kawatake, M. Murata, O. Nureki, S. Owada, T. Kameshima, T. Hatsui, Y. Joti, G. Schertler, M. Yabashi, A.-N. Bondar, J. Standfuss, R. Neutze and S. Iwata, *Science*, 2016, **354**, 1552–1557.

5 (*a*) S. R. Tachibana, L. Tang, L. Zhu, W. Liu, Y. Wang and C. Fang, *J. Phys. Chem. B*, 2018, **122**, 11986–11995; (*b*) M. H. Lee, J. S. Kim and J. L. Sessier, *Chem. Soc. Rev.*, 2015, **44**, 4185–4191.

6 (*a*) X.-C. Chen, T. Tao, Y.-G. Wang, Y.-X. Peng, W. Huang and H.-F. Qian, *Dalton Trans.*, 2012, **41**, 11107–11115; (*b*) J. Cai, Z. Li, Y. Qiu, Z. OuYang, W. Lin, L. Yang, W. Feng, X. Yu and W. Dong, *New J. Chem.*, 2016, **40**, 9370–9379; (*c*) J. Cheng, D. Liu, W. Li, L. Bao and K. Han, *J. Phys. Chem. C*, 2015, **119**, 4242–4251.

7 (*a*) D. McMorrow and M. Kasha, *J. Phys. Chem.*, 1984, **88**, 2235–2243; (*b*) X. Zhao, X. Li, S. Liang, X. Dong and Z. Zhang, *RSC Adv.*, 2021, **11**, 28851–28862; (*c*) X. Bi, B. Liu, L. McDonald and Y. Pang, *J. Phys. Chem. B*, 2017, **121**, 4981–4986.

8 (*a*) H. Wang, Y. Xiao, Z. Xie, H. Sun, X. Zhang, J. Wanga and R. Huang, *Front. Chem.*, 2021, **9**, 766179; (*b*) M. T. Ignasiak, C. Houée-Levin, G. Kciuk, B. Marciniak and T. Pedzinski, *ChemPhysChem*, 2015, **16**, 628–633.

9 (*a*) P. F. Barbara, L. E. Brus and P. M. Rentzepis, *J. Am. Chem. Soc.*, 1980, **102**, 5631–5635; (*b*) S. Pijeau, D. Foster and E. G. Hohenstein, *J. Phys. Chem. A*, 2017, **121**, 4595–4605; (*c*) S. Barman, S. K. Mukhopadhyay, M. Gangopadhyay, S. Biswas, S. Dey and N. D. P. Singh, *J. Mater. Chem. B*, 2015, **3**, 3490–3497.

10 X. Zhang, L. Guo, F.-Y. Wu and Y.-B. Jiang, *Org. Lett.*, 2003, **5**, 2667–2670.
11 I. Presiado, Y. Erez, R. Gepshtein and D. Huppert, *J. Phys. Chem. C*, 2010, **114**, 3634–3640.
12 K. Togasaki, T. Arai and Y. Nishimura, *J. Phys. Chem. A*, 2020, **124**, 6617–6628.
13 (*a*) M. Miura, J. Harada and K. Ogawa, *J. Phys. Chem. A*, 2007, **111**, 9854–9858; (*b*) S. Slavova and L. Antonov, *Phys. Chem. Chem. Phys.*, 2024, **26**, 7177–7189.
14 (*a*) K. Sakota, A. Hara and H. Sekiya, *Phys. Chem. Chem. Phys.*, 2004, **6**, 32–36; (*b*) X.-f. Yu, S. Yamazaki and T. Taketsugu, *Phys. Chem. Chem. Phys.*, 2017, **19**, 23289–23301.
15 (*a*) K. Ogawa, M. Miura, T. Nakayama and J. Harada, *Chem. Lett.*, 2003, **32**, 840–841; (*b*) D. L. Wisman, H. Kim, C. Kim, T. W. Morris, D. Lee and S. L. Tait, *Chem. – Eur. J.*, 2021, **27**, 13887–13893.
16 (*a*) C. Tanner, C. Manca and S. Leutwyler, *Science*, 2003, **302**, 1736–1739; (*b*) O.-H. Kwon, Y.-S. Lee, B. K. Yoo and D.-J. Jang, *Angew. Chem., Int. Ed.*, 2006, **45**, 415–419; (*c*) Y. Matsumoto, T. Ebata and N. Mikami, *J. Phys. Chem. A*, 2002, **106**, 5591–5599; (*d*) P.-T. Chou, C.-Y. Wei, C.-R. C. Wang, F.-T. Hung and C.-P. Chang, *J. Phys. Chem. A*, 1999, **103**, 1939–1949.
17 K. Ohira, M. Yamamoto, K. Imato and Y. Ooyama, *New J. Chem.*, 2023, **47**, 2711–2718.
18 (*a*) K. Takagi, A. Mizuno, H. Yoshimura and M. Matsuoka, *Dyes Pigm.*, 1990, **14**, 203; (*b*) K. Imato, K. Ohira, M. Yamaguchi, T. Enoki and Y. Ooyama, *Mater. Chem. Front.*, 2020, **4**, 589–596; (*c*) K. Ohira, K. Imato and Y. Ooyama, *Mater. Chem. Front.*, 2021, **14**, 5298–5304.
19 (*a*) I. Yosioka and H. Otomasu, *Pharm. Bull.*, 1954, **2**, 53–59; (*b*) C. Seillan, H. Brisset and O. Siri, *Org. Lett.*, 2008, **10**, 4013–4016.
20 (*a*) T.-B. Wei, W.-T. Li, Q. Li, J.-X. Su, W.-J. Qu, Q. Lin, H. Yao and Y.-M. Zhang, *Tetrahedron Lett.*, 2016, **57**, 2767–2771; (*b*) C. Grieco, A. T. Hanes, L. Blancafort and B. Kohler, *J. Phys. Chem. A*, 2019, **123**, 5356–5366.
21 C. Seillan, P. Marsal and O. Siri, *Org. Biomol. Chem.*, 2010, **8**, 3882–3887.
22 (*a*) S.-H. Liu, R.-L. Guo, W.-C. Chen, H.-Y. Hou and C.-M. Shu, *J. Loss Prev. Process Ind.*, 2021, **70**, 104403; (*b*) X.-R. Li, X.-L. Wang and H. Koseki, *J. Hazard. Mater.*, 2008, **159**, 13–18.
23 (*a*) J. Harada, T. Fujiwara and K. Ogawa, *J. Am. Chem. Soc.*, 2007, **129**, 16216–16221; (*b*) T. Fujiwara, J. Harada and K. Ogawa, *J. Phys. Chem. B*, 2004, **108**, 4035–4038; (*c*) T. Fujiwara, J. Harada and K. Ogawa, *J. Phys. Chem. A*, 2009, **113**, 1822–1826; (*d*) J. Harada, H. Uekusa and Y. Ohashi, *J. Am. Chem. Soc.*, 1999, **121**, 5809–5810; (*e*) K. Ogawa and J. Harada, *J. Mol. Struct.*, 2003, **647**, 211–216; (*f*) J. Harada and K. Ogawa, *Chem. Soc. Rev.*, 2009, **38**, 2244–2252; (*g*) K. Ogawa and T. Fujiwara, *Chem. Lett.*, 1999, **28**, 657–658; (*h*) K. Ogawa, J. Harada, I. Tamura and Y. Noda, *Chem. Lett.*, 2000, **29**, 528–529; (*i*) K. Ogawa, Y. Kasahara, Y. Ohtani and J. Harada, *J. Am. Chem. Soc.*, 1998, **120**, 7107–7108.
24 M. J. Frisch, G. W. Trucks, H. B. Schlegel, G. E. Scuseria, M. A. Robb, J. R. Cheeseman, G. Scalmani, V. Barone, G. A. Petersson, H. Nakatsuji, X. Li, M. Caricato, A. V. Marenich, J. Bloino, B. G. Janesko, R. Gomperts, B. Mennucci, H. P. Hratchian, J. V. Ortiz, A. F. Izmaylov, J. L. Sonnenberg, D. Williams-Young, F. Ding, F. Lipparini, F. Egidi, J. Goings, B. Peng, A. Petrone, T. Henderson, D. Ranasinghe, V. G. Zakrzewski, J. Gao, N. Rega, G. Zheng, W. Liang, M. Hada, M. Ehara, K. Toyota, R. Fukuda, J. Hasegawa, M. Ishida, T. Nakajima, Y. Honda, O. Kitao, H. Nakai, T. Vreven, K. Throssell, J. A. Montgomery Jr., J. E. Peralta, F. Ogliaro, M. J. Bearpark, J. J. Heyd, E. N. Brothers, K. N. Kudin, V. N. Staroverov, T. A. Keith, R. Kobayashi, J. Normand, K. Raghavachari, A. P. Rendell, J. C. Burant, S. S. Iyengar, J. Tomasi, M. Cossi, J. M. Millam, M. Klene, C. Adamo, R. Cammi, J. W. Ochterski, R. L. Martin, K. Morokuma, O. Farkas, J. B. Foresman and D. J. Fox, *Gaussian 16, Revision B.01*, Gaussian, Inc., Wallingford CT, 2016.